Variation in Cosmic Ray Count Rate at Doi Inthanon with Atmospheric Water Vapor

P. Muangha*, P.-S. Mangeard, D. Ruffolo and A. Sáiz

Department of Physics, Faculty of Science, Mahidol University, 272 Rama VI Road, Phayathai, Ratchathewi, Bangkok, 10400

*E-mail: Fhoone@hotmail.com

Abstract

The *Princess Sirindhorn Neutron Monitor* (*PSNM*) at Doi Inthanon, Thailand provides important information about high-energy cosmic rays from space. Both the neutron monitor (NM) and Bare (lead-free) neutron counters detect the variation of intensity in the interplanetary cosmic rays. In addition, the bare detector to neutron monitor count rate ratio (BNM) provides information on the particle spectrum. We found that variation in BNM is strongly anti-correlated with atmospheric water vapor (E_w) as inferred from the Global Atmospheric Data Assimilation (GDAS). In the present work, we develop a correction to Bare/NM for water vapor pressure. The results of comparison of the E_w from the GDAS database with another database will be discussed.

Keywords: Neutron monitor, Cosmic rays

Introduction

Neutron monitors are ground-based detectors for measuring Galactic cosmic ray (GCRs) by detecting atmospheric secondary particles. Those secondary particles are produced by the interaction of primary cosmic ray in the Earth's atmosphere. The neutron monitor count measuring the time variation of GCR flux over 22 year solar magnetic cycles, 11-year sunspot cycles, Sun's 27-day rotation period, Earth's 1-day rotation period [2,3,5,7,9]. Time variations in the cosmic ray provide important information about solar energetic particles from solar storms [11,12] and effects on the Galactic cosmic-ray (GCR) due to solar activity, coronal mass ejections, solar wind.

At any given location the Earth's magnetic field excludes cosmic ray from their rigidity ($P = pc/q$), where p is momentum and q is particle charge). The vertical geomagnetic cutoff varies from 1 GV to 17 GV. The cosmic ray primary energy must exceed an atmospheric cutoff rigidity to be detectable at ground level. Neutron monitor station worldwide the GCR spectrum from a comparison of NM count rates at varying cutoff rigidity [6].

The *PSNM* is located at Doi Inthanon, Thailand at an altitude of about 2560m and geographic coordinates 18°.95N and 98°.49E, with the world's highest vertical geomagnetic cutoff rigidity of 16.8 GV. This study used cosmic ray data from the *PSNM* which houses an 18-tube neutron monitor, standard NM64 [4], and 3-tube bare counter, without reflector and lead producer. There are detect the secondary neutron in different energy. Neutron monitor detect high energy neutron and bare counter detect low energy neutron. The bare to neutron monitor count rate ratio (BNM) provide information of cosmic ray spectral variation.

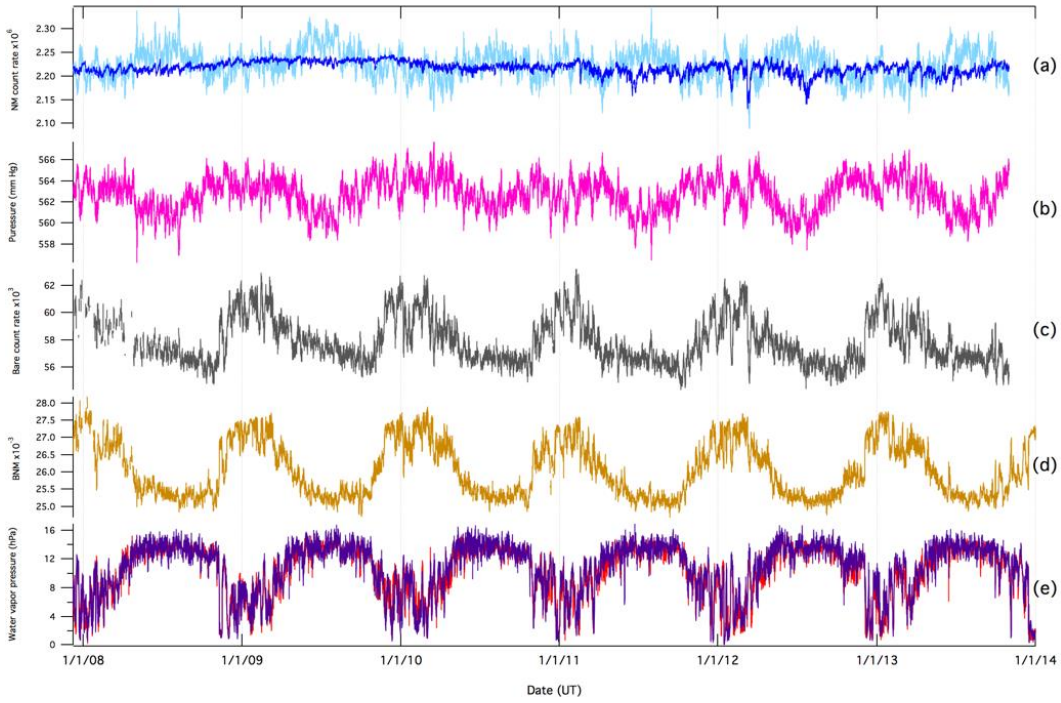

Figure 1 The data for Doi Inthanon from 2007 December to 2013 December: (a) neutron monitor count rate, uncorrected (light blue) and corrected (dark blue) for atmospheric pressure. The neutron monitor count rate with for pressure is indicate the the variation in Galactic cosmic ray flux associated with the solar activity. (b) Atmospheric pressure (*p*) at *PSNM* station. (c) Bare count rate measure low-energy secondary neutron. (d) Count rate ratio of bare to neutron monitor variation is anti-correlation with atmospheric water vapor pressure. (e) Atmospheric water vapor pressure (E_w) from GDAS database (red) and MERRA-2 database (violet).

Materials and Methods

Observations and Data Analysis

In order to study the variations of the primary cosmic rays, the atmospheric effects on the secondary neutron observed by ground-based detectors must be considered. Although the barometric effect correction for neutron monitor, in which atmospheric pressure at the level already known, is defined as an exponential relationship with barometric pressure:

$$C_{\text{Corrected}} = C_{\text{Uncorrected}} exp(\beta(P - P_{\text{ref}})$$

where P is atmospheric pressure (mmHg) an P_{ref} is the reference atmospheric pressure (mmHg) and β is the atmospheric coefficient for neutron secondary cosmic rays, at Doi Inthanon a pressure coefficient β = 0.854% mmHg^{-1} and standard pressure P_0 = 563 mmHg

Neutron intensity above the surface is related to the contribution of hydrogen [10]. Then we have investigated a possible dependence of the BNM ratio on atmospheric water vapor pressure, E_w by comparison with data from the Global Atmospheric Data Assimilation (GDAS) database, which is available from *http://ready.arl.noaa.gov/gdas1.php*, and the Modern-Era Retrospective analysis for Research and Applications, Version 2 (MERRA-2) database, which is available from *http://disc.sci.gsfc.nasa.gov/mdisc*. We use the relative humidity *H* (in %) and *T* (in °C) for

a pressure level of 750 hPa at the four surrounding special grind points and interpolate these to geographic location of *PSNM*. We use formula:

$$E_w = 4.585\frac{H}{100}\exp\left(\frac{17.62T}{T+243.12}\right)\ \text{mmHg}$$

to infer the atmosphere water vapor pressure E_w [1,8]. The GDAS data are available at 6-hour interval, but MERRA-2 data are available at 3-hour interval. So we use 6-hour average interval for GDAS and MERRA-2.

We found that the yearly variation in the uncorrected BNM is well explain by the effect of water vapor pressure (E_w). The pressure has a yearly variation and also has 24-hour and 12-hour variation due to the Earth's rotation but E_w still unclear in short term variation. We use these short-term variations to remove the atmospheric effect.

In this part, we performed a linear regression to find correlation of the BNM with pressure and water vapor pressure, in which GDAS and MERRA-2. We obtained regression coefficient of (0.08 ± 0.03) x10^{-3} hPa^{-1} and – (1.11 ± 0.05) x10^{-3} hPa^{-1} and – (1.52 ± 0.03) x10^{-3} hPa^{-1}, for pressure, E_w from GDAS, and E_w from MERRA-2, respectively. The pressure has a small effect on BNM but water vapor pressure is higher.

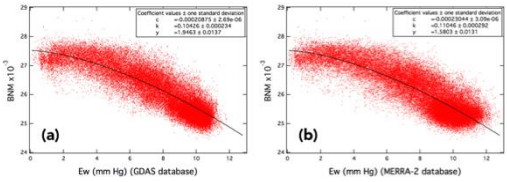

Figure 2 Correlation between BNM and E_w for GDAS database (a). Correlation between BNM and E_w for MEARRA-2 database (b).

For correct effect of water vapor, the correlation between BNM and E_w is nonlinear dependence. There are strongly anti-correlated at high E_w. We fit the BNM versus E_w to a power law:

$$BNM \sim BNM(E_{W,0})\left[\frac{1-k(E_w^{\gamma}-E_{w,0}^{\gamma})}{(12\ \text{mmHg})}\right]$$

We obtain $k \sim 0.104$, 0.110 and $\gamma \sim 1.94$, 1.58 for GDAS database and MERRA-2 database. Then we can correct BNM for atmospheric water vapor pressure by dividing it by the term in square brackets.

Results and Discussion

The vapor corrected BNM for water vapor pressure E_w, Figure 3(a), has obvious non-effect of water vapor pressure. We believed that these corrected BNM are relate to the primary cosmic ray. In short-term variation, the water vapor pressure data from GDAS database and MERRA-2 database are different. The water vapor pressure (E_w) from MERRA-2 has a higher fluctuate and E_w from GDAS database is a better correlation with BNM.

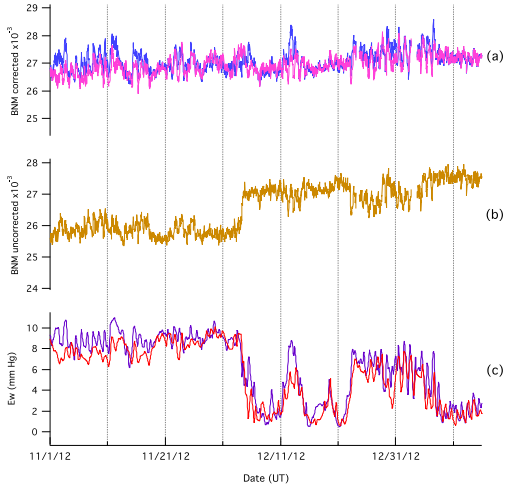

Figure 3 The data from 2012 November to 2013 January: (a) The BNM ratio corrected for atmospheric water vapor pressure from GDAS database (pink) and MERRA-2 database (blue). (b) Uncorrected BNM ratio measure at the *PSNM* station. (c) Atmospheric water vapor pressure (E_w) inferred from the GDAS database (red) and MERRA-2 database (violet).

The vapor corrected BNM has a diurnal (a daily) variations. The daily variation in vapor corrected BNM is correlated with the Earth's rotation and anti-correlation to temperature inside the PNM station. For daily variation we found the temperature coefficient in 0.168% ($°C^{-1}$) and 0.078% ($°C^{-1}$) for GDAS database (pink) and MERRA-2 database (blue).

Conclusions

Seasonal variations in Galactic cosmic ray spectral variation, indicate by bare/NM ratio, are best explained by the effect of atmospheric water vapor pressure (E_w). The atmospheric water vapor pressure from GDAS database is greater correlate with BNM than MERRA-2 database. After correcting these effect, the vapor corrected BNM has a daily variation due to the Earth's rotation.

Acknowledgments

Supported partial by faculty of Graduate Studies, Mahidol university, Thailand.

References

[1] Aiemsa-ad, et al. (2015). Measurement and simulation of neutron monitor count rate dependence on surrounding structure. ***JGRA***, *120*, 5253.

[2] Forbush, S.E. (1954). World-wide cosmic-ray variations, 1937-1952. *JGR, 59*, 525.

[3] Gleeson L.J. and Axford W.I. (1968). Solar modulation of galactic cosmic rays. *ApJ, 154*, 1011.

[4] Hatton C.J. and Carmichael H. (1964). Experimental investigation of the NM-64 neutron monitor. *Can. J. Phys., 42*, 2443.

[5] Jokipii J.R. and Thomas B. (1981). Effects of drift on the transport of cosmic rays. IV - Modulation by a wavy interplanetary current sheet. *ApJ, 243*, 1115.

[6] Moraal H., Belov A. and Clem J.M. (2000). Design and co-ordination of multi-station international neutron monitor networks. *SSRv, 93*, 285.

[7] Nuntiyakul W., et al. (2014). Latitude survey investigation of galactic cosmic ray solar modulation during 1994-2007. *ApJ, 795*, 11.

[8] Ruffolo D., et al. (2016). Monitoring short-term cosmic-ray spectral variations using neutron monitor time-delay measurements. *ApJ, 817*, 38.

[9] Yeeram T., et al. (2014). Corotating solar wind structures and recurrent trains of enhanced diurnal variation in galactic cosmic rays. *ApJ, 784*, 136.

[10] Zreda M., et al. (2008). Measuring soil moisture content non-invasively at intermediate spatial scale using cosmic-ray neutrons. *Geophys. Res. Lett., 35*, L2140.

[11] Bieber J.W., et al. (2013). Giant Ground Level Enhancement of Relativistic Solar Protons on 2005 JANUARY 20.I. Spaceship Earth Observations. *ApJ, 771*, 92.

[12] Meyer P., et al. (1956). Solar Cosmic Rays of February, 1956 and Their Propagation Through Interplanetary Space. *Phys. Rev. 104*, 768.

Umbra and Penumbra Areas of Sunspot from the Solar and Heliospheric Observatory Image

T. Sudjai*

Department of Physics, Mahidol Wittayanusorn School, Salaya, Phuttamonthon Nakorn Pathom, 73170

*E-mail: thawatchai@mwit.ac.th

Abstract

The areas of umbra and penumbra of sunspots can indicate the magnetic field of the sun, and the development of the sunspot groups. As the size of umbra and penumbra areas depend on the intensity of the magnetic field, the records of these areas are very important. The pair of sunspot members from opposite magnetic polarity relate to the extension of the areas of umbra, penumbra and group of sunspot areas. In this study, a pixel count in the sun digital imaging from the solar and heliospheric observatory, NASA, is used. Since the umbra and penumbra have different levels of light intensity. The image processing program can be used to identify the intensity of the black color of the sun digital image. In mode of grey scale, the percentage of the black color is measured. The increase and decrease between the areas of umbra and penumbra are very obvious. The relative of it to the magnetogram data is very distinctly correlation both of the sunspot pair and others.

Keywords: Sunspot, Umbra, Penumbra

Introduction

The sunspot areas are the most important part of the growth and decomposition of sunspot groups [1]. They have lower temperatures, as collated to the surrounding photosphere [4]. The areas of sunspots are associated with a solar magnetic field structure [4]. The ratio of penumbral area to umbral area in a sunspot group allow us to understand the formation of umbra and penumbral and some properties of the sun [2]. For a long time, over nearly 150 years, it has been observed that the diverse areas of the numbers of sunspot groups change with time [5]. However, to enhance solar database, the development of sunspot database is still benefit and very significance. Matching the non-overlapping solar active-region nomenclature is one way to do in many studies [3]. In this study, a heliographic coordinate system method is used to measure true areas of the sunspots.

Materials and Methods

The first step, is to measure the area of sunspot by collecting images from the Solar and Heliospheric Observatory Images (Figure 1), and then select the clear images of sunspot groups which are suitable for analysis of sunspot areas. The selected ones in this work are the pair of sunspot A and sunspot B in group 2371 (Figure 2). After that, we use image processing program to transform the images to grayscale and adjust the level of intensity for separating between umbra and penumbral clearly and easily. Finally, the different intensity levels of black color of umbra (black) and penumbral (gray) are suitable for analysis (Figure 3).

The second step, is to calculate the heliographic coordinates of a pixel. Due to its 2 dimensional image, it must be transformed to 3 dimensional coordinates

system first. And then using the relation between the Cartesian and heliographic coordinates, the true areas of umbra, penumbral and sunspot are possible to calculate in degree of area.

The transformation can be done as follows: When x and z are the positions of the pixel P from the center of the sun in 2 dimensional image and r is radius of the solar disk image, the heliographic coordinates of the pixel, L_p and B_p, are obtained in degrees by

$$B_p = \arcsin\left(\frac{z}{r}\right)\frac{180}{\pi}$$

$$L_p = \arctan\left(\frac{x}{rcos(90-B_p)}\right)\frac{180}{\pi}$$

where B_p and L_p are the latitude angle and longitude angle at point P, respectively. And also, the heliographic coordinates of the nearest pixel of point P must be calculated. Then, with all these available data the true areas can be calculated.

Finally, the sun magnetogram images (Figure 4) are overlaid on the solar images by using the computer graphic program (Figure 5). Therefore the comparison and conclusion about the area of umbra, penumbra and sunspot can be done.

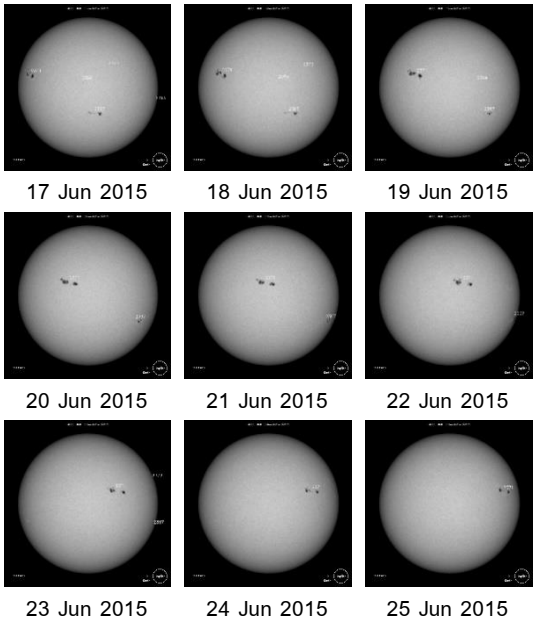

Figure 1 Solar images supported by SOHO observatory (Solar and Heliosphere Observatory).

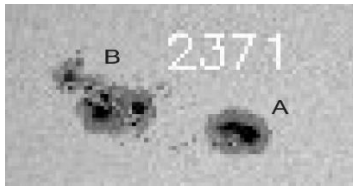

Figure 2 A pair of sunspot A and B in group 2371

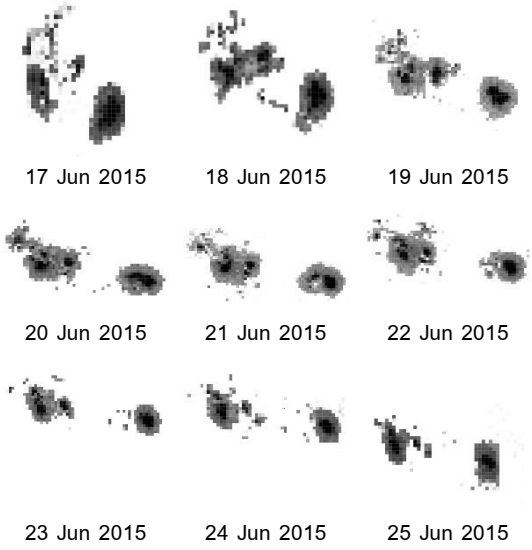

Figure 3 Sunspot images.

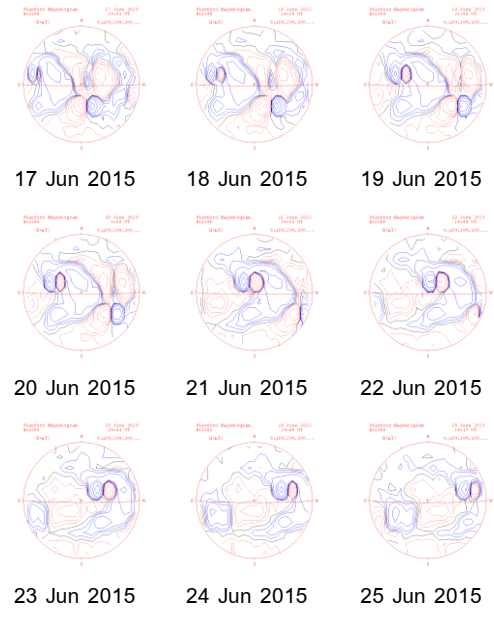

Figure 4 The Sun magnetogram images supported by Stanford Solar Center.

Results and Discussion

The calculated results in heliographic coordinates and areas of sunspot group 2371 during 17 – 25 June 2015 are expressed in Table 1. It shows that on 17 June 2015 the maximum umbra area of sunspot A is 3.09 degree^2 and the minimum one of sunspot B is 1.07 degree^2. Additionally, on 22 June 2015 the maximum of penumbral area of sunspot B is 29.37 degree^2 and on 24 June 2015 the minimum one of sunspot A is 6.16 degree^2. Whilst the total sunspot areas of all sunspot group 2371 during 17 to 25 June 2015 are not constant, the maximum one is 52.02 degree^2 on 22 June 2015, and the minimum one is 17.04 degree^2 on 19 June 2015.

Table 1 The calculated results of areas

Date	Umbra area $(^\circ)^2$ (A/B)	Penumbra area $(^\circ)^2$ (A/B)	Total Sunspot Area $(^\circ)^2$
2015.06.17	3.09/1.07	8.34/9.96	22.46
2015.06.18	2.42/2.43	9.66/19.31	33.82
2015.06.19	1.74/1.79	6.91/6.60	17.04
2015.06.20	1.42/2.17	7.03/18.85	29.47
2015.06.21	1.45/1.61	7.87/17.40	28.33
2015.06.22	2.81/3.29	16.55/29.37	52.02
2015.06.23	1.85/1.56	6.88/8.29	18.58
2015.06.24	1.31/1.54	6.16/8.81	17.82
2015.06.25	1.57/1.41	9.87/6.88	19.73

The average ratio of penumbra/umbra area on sunspot A and B is 4.63 and 7.26, respectively. The maximum ratio is 10.82 on sunspot B on 21 June 2015 and the minimum ratio is 2.70 on sunspot A on 17 June 2015 (Table 2).

In case of the overlay of sun magnetogram image on the solar image (Figure 5), it can be observed that there is very strong magnetic field of sun around the area of sunspot. Additionally, from Figures 1 and 4, it can be confirmed that this phenomenon appears the same in all 9 day-imanges.

Table 2 Ratio of penumbral/umbra area.

Date	A : Ratio of Penumbral/ Umbra area	B : Ratio of Penumbral/ Umbra area
2015.06.17	2.70	9.33
2015.06.18	4.00	7.96
2015.06.19	3.96	3.70
2015.06.20	4.96	8.69
2015.06.21	5.44	10.82
2015.06.22	5.89	8.92
2015.06.23	3.72	5.30
2015.06.24	4.71	5.74
2015.06.25	6.27	4.87

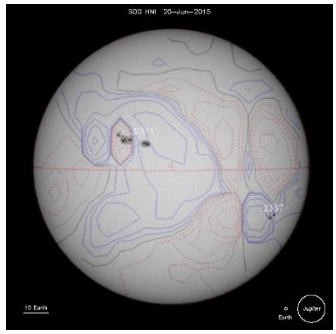

Figure 5 The overlay of Sun magnetogram image on the solar image on 20 June 2015.

Conclusions

In this work, the pair of sunspot A and B in group 2371 during 17 to 25 June 2015 were selected to study. From the results in Table 1, it can be concluded that the maximum area of sunspot group 2371 is 52.02 degree^2 and the minimum one is 17.04 degree^2 and obviously areas of sunspot group correlated to their lifetime. In this work, it is not possible to see the trend of the relationship of the variability between umbra area and penumbral area, since the study period was too short. Consequently, for the near future of the study in this topic, it should be set the study period which is long enough to be able to observe such trend as mentioned before. Additionally, from Table 2 the average ratio of

penumbral area to umbra area of sunspot group 2371 is 5.94. It means that normally penumbral area is probably larger than umbra area and both penumbral and umbra area have clearly different levels of light intensity. With these results, it also shows the feasibility of this technique for area analysis of both umbral and penumbral. Importantly, from the overlay imanges, the relation between sunspot group and the solar magnetogram data is very distinctly correlated, which is able to reveal obviously strong solar magnetic field on the sun spot areas.

Acknowledgments

Thanks very much to SOHO observatory (Solar and Heliosphere Observatory) and Stanford Solar Center for supporting solar images and the solar magnetograms images.

References

[1] Cakmak H. (2014). A Digital Method to Calculate the True Areas of Sunspot Groups. *Exp Astron., 37,* 539-553.

[2] Hathaway D.H. (2013). A Curious History of Sunspot Penumbrae. *Solar Phys., 286,* 347-356.

[3] Laure L. and Frederic C. (2014). Survey and Merging of Sunspot Catalogs. *Solar Phys., 289,* 545-561.

[4] Ragadeepika P., Hiremath K.M. and Shashanka R.G. (2016). Development of a Code to Analyze the Solar White-Light Imanges from the Kodaikanal Observatory: Detection of Sunspots, Computation of Heliographic Coordinates and Area. *Astrophys:Astr., 37*, 3.

[5] Obridko V.N. and Badalyan O.G. (2014). Cyclic and Secular Vaiations Sunspot Groups with Various Scales. *Astronomy Reports., 58(12),* 936-944.

Wireless Ticker as a Learning Tool in Physics

K. Chongcharoen*, W. Putchana, M. Deeudom, S. Im-erb and A. Ratanavis

Department of Industrial Physics and Medical Instrumentation, Faculty of Applied Science, Lasers and Optics Research Group (LANDOS), Science and Technology Institute, King Mongkut's University of Technology North Bangkok, Bangkok, Thailand

*E-mail: Chong.Kanokwan@gmail.com

Abstract

This paper presents a further development of a so-called Ticker, a device supporting "hear and see" activity in classroom or laboratory exercises. While the original version of Ticker performs as a timing device, a new version of Ticker is improved in the sense of fast and wireless timing device. This wireless version provides the flexibility of measurements in various physics problems. The wireless ticker composes of a photodiode, a simple circuit, a wireless transmitter and a buzzer. The photodiode is equipped to enable the fast rise time. The ticker is operated by the change of intensity of the detected light on its photodiode. The simple circuit sends the signal through the transmitter while the wireless receiver is connected to a personal computer. Our developed software can be used to analyze the received signal. This new features of the ticker are meant to fulfill challenges in various teaching environments. The wireless ticker can also generate the ticking sound that aims to accommodate students with visual impairments. The experiments on simple harmonics, simple pendulum and acceleration have been performed as examples to show the capability of the wireless ticker. The demonstration shows the promise of the wireless ticker as a new teaching tool. This economic device allows a huge room for creativity with simplicity of reliable measurements.

Keywords: Light sensors, Lasers, Physics demonstrations

Introduction

In large classroom environments, learning of students reveals problems in the sense of attention and participation especially on traditional lectures in physics [1-5]. Based on research on physics education, the curriculum development can alleviate such a problem [4]. In addition, lecture demonstrations have been proven to support the development [6-8].

In recent years, the demonstration based-exercise (DBE) project has been proposed as alternative approach to support lecture demonstrations and activities in class lectures [9]. As a consequence, the DBE project is being developed in the department of industrial physics and medical instrumentation, King Mongkut's University Technology of North Bangkok to enhance student participation and attention.

During the development of the DBE project, a so called "ticker" device was proposed as a timing device to support learning activities based on demonstrations [9].

Despite successes, there is still a room of further development. The development of ticker aims to flexibility, fast response for data collection, and economic cost. A so called "wireless ticker" is meant to be introduced in this paper. This current version of ticker can be used in various experiments. However, in this contribution the experiments on simple harmonics, simple pendulum and acceleration were performed to examine the capability of wireless ticker.

These demonstrations can be used to illustrate the performance of wireless ticker and guide us to further possible experiments in physics.

Materials and Methods

As shown in Figure 1, the operation principle of ticker is based on the variation of light intensity. The light source can be a LED or lasers sending the optical signal to the light sensor. The microcontroller is designed to receive and send the electronic signal to the Xbee served as the wireless sending signal device.

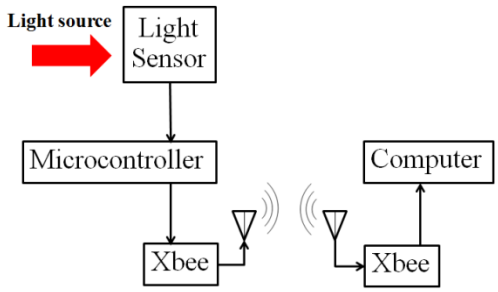

Figure 1 Operating components of wireless ticker.

The wireless receiver made by Xbee is meant to receive the wireless signal and transfer the signal to a developed software that was designed for the data collection. Figure 2 shows the wireless ticker with its software.

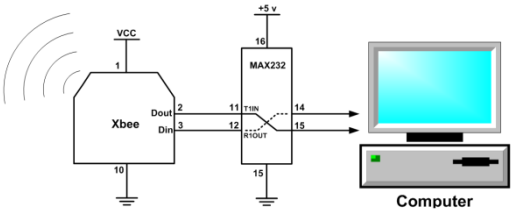

Figure 2 Wireless ticker and the ticker's software.

The use of wireless ticker can be demonstrated by using varoius physics experiments which are a simple pendulum, simple harmonic motion of spring and accerleration. In these experiments, wireless ticker can be used as the timing device and the object under the investigation. Figure 3 shows the setup of these experiments. HeNe lasers was served as the light source for the wireless ticker. In these experiments, the motion of the wireless ticker plays as an important role for the optical measurements. The signal captured by the wireless receiver is displayed on the ticker 's software. The experimental data can be collected in real time.

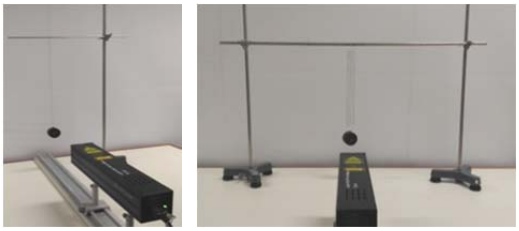

(a) (b)

(c)

Figure 3 Experiments on simple pendulum, simple harmonic motion and accerelation.

The description of these experiments can be found elsewhere. It should be mentioned that the time scale of the data collection was in the order of milliseccond (ms).

For the simple pendulum, the wireless ticker serves as a small bob suspended by a cord. The wireless ticker was freely released to swing in the manner of simple harmonic motion.

In the case of the spring vibration experiment, the wireless ticker acts as the mass hanging on a spring.

For the acceleration experiment, the wireless ticker plays as the light sensor and mass under the observation.

Results and Discussion

Figure 4 shows the plot between the cord length (L) and the square of the period (T^2). The slope of the plot was 0.25 m/s^2. This result reveals the acceleration due to the gravity on the surface of earth (g) that is 9.87 m/s^2.

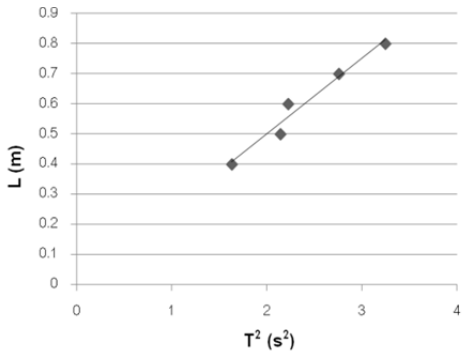

Figure 4 The relation between the cord length (L) and the square of the period (T^2) obtained by the experiment on simple pendulum.

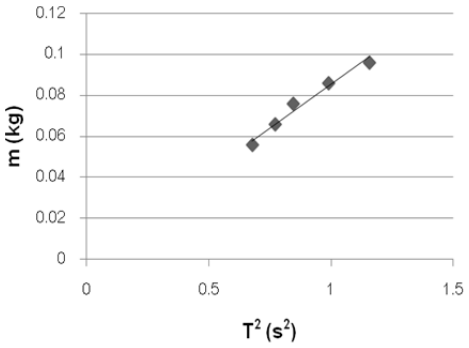

Figure 5 The relation between the mass (m) and the square of the period (T^2) obtained by the experiment on simple harmonic motion.

Figure 5 shows the relation between the mass (m) and the square of the period (T^2) provided by the oscillation of the vertical spring. According of the graph, the spring constant was 3.35 N/m.

Based on the acceleration experiment, the acceleration of the moving objects can be determined. The value of 2.9 m/s^2 is compable to the calculation.

Conclusion

In this research, the wireless ticker is proposed to support real-time demonstrations in physics and experimental exercises. As a wireless timing device, the wireless ticker has a great potential to conduct experiments with simplicities of setup and measurement.

Furthermore, the wireless ticker can be used as a part of an economic approach to stimulate the interactive lecture demonstrations (ILDs) strategies. The simple pendulum, harmonic motion and acceleration experiments are excellent examples of the use of the wireless ticker. The wireless ticker can provide motivation and conceptual learning to students. It is evident that there is a huge room of creativity for the wireless ticker as a teaching tool in physics.

Acknowledgments

This research work is financially supported by Faculty of Applied Science, King Mongkut's University of Technology North Bangkok under Grant No. 5743107.

References

[1] McDermott L. and Redish E. (1999). Resource letter PER-1: physics education research. *Am. J. Phys., 67*, 755.

[2] Keiner L. and Burns T. (2010). Interactive engagement: how much is enough?. *Phys. Teach., 48*, 108.

[3] Gonzalez M., et al. (2002). Development of a virtual laboratory on the internet as support for physics laboratory training. *Eur. J. Phys., 23*, 61.

[4] Redish E. (2003). Teaching physics with physics suite. *Wiley*.

[5] Crouch C., et al. (2004). Classroom demonstrations: Learning tools or entertainment?. *Am. J. Phys., 72,* 835.

[6] Spike B. and Finkelstein N. (2012). Preparing tutorial and recitation instructors: A pedagogical approach to focusing attention on content and student reasoning. *Am. J. Phys., 80,* 1020.

[7] Anderson J. and Barnett M. (2011). Using video games to support pre-service elementary teachers learning of basic physics principles. *J. Sci. Educ. Technol., 20*, 347.

[8] Sharma M., et al. (2010). Use of interactive lecture demonstrations: A ten year study. *Phys. Rev. ST Physics Ed. Research, 6*, 020119.

[9] Leevongwat P., et al. (2013). A Development of the Demonstration Based-exercise Project. The Siam Physics Congress 2013.

The Comparative Effect of Reliability to Integrated Circuit (IC) Package between Conventional Oven Cure and Pressure Oven Cure Process

A. Noinongyao[1*], P. Thonglor[1], K. Ugsornrat[1] and C. Sumithpibul[2]

[1]Department of Industrial Physics and Medical Instrumentation, Faculty of applied Science, King Mongkut's University of Technology North Bangkok, 10800

[2]Department of Engineering, UTAC Thai Limited, Bangkok, 10260

*E-mail: Ameena.noinongyao@gmail.com

Abstract

This research studied about the efficiency of conventional oven and pressure oven of epoxy curing after die attach process to integrated circuit (IC) packaging reliability. Epoxy curing process is so important to make a completed epoxy due to cross linking to enhance microstructure of epoxy stiffness. This experiment, the samples were tested for two types of non conductive die attach screen print and were cured for conventional oven cure and pressure oven cure. In general process of oven cure to dry epoxy is using a conventional oven but a void can still occur in the layer of epoxy. Therefore, pressure oven cure used for reduction the void that has effect to the reliability of IC package. For analysis, 5x5 mm^2 of QFN packages were analyzed by die shear test and were also tested by moisture sensitive level (MSL) to observe void inside the packages. The results showed that the pressure oven cure can be reduced void inside the package and improved IC packaging reliability.

Keywords: Integrated circuit (IC) packaging, Non conductive epoxy, Die attach screen print, Conventional oven cure, Pressure oven cure

Introduction

Die attach process is one that is very important in the integrated circuit (IC) packaging manufacturing. This process is the attaching a die or chip take to substrate or package. There are several methods for attaching die onto leadframe. Epoxy curing process is so important to make a completed epoxy due to cross linking to enhance microstructure of epoxy stiffness. This experiment, the samples were tested for two types of non conductive die attach screen print and were cured for conventional oven cure and pressure oven cure. In general process of oven cure to dry epoxy is using a conventional oven but a void can still occur in the layer of epoxy. Therefore, pressure oven cure used for reduction the void that has effect to the reliability of IC package.

Therefore, this research the Comparative Effect of Reliability between Conventional Oven Cure and Pressure Oven Cure Process. Can be reduced void inside the package and improved IC packaging reliability.

Materials and Methods

In this study, built unit with 5×5 mm package size. Die Size(mil) /Epoxy is 75x75. Die attach process parameters have been setup in previous work. The samples were tested for two types of non conductive die attach screen print and were cured for conventional oven cure and pressure oven cure.

Table 1 Comparison of between Oven type.

Package Structure	5x5 mm
Die Size (mil) /Epoxy	75x75
Epoxy type	Screen print
Oven type	- Conventional oven - Pressure oven

For analysis, the sample were tested for two types cured for conventional oven cure and pressure oven cure for die shear, and moisture sensitivity level (MSL) test

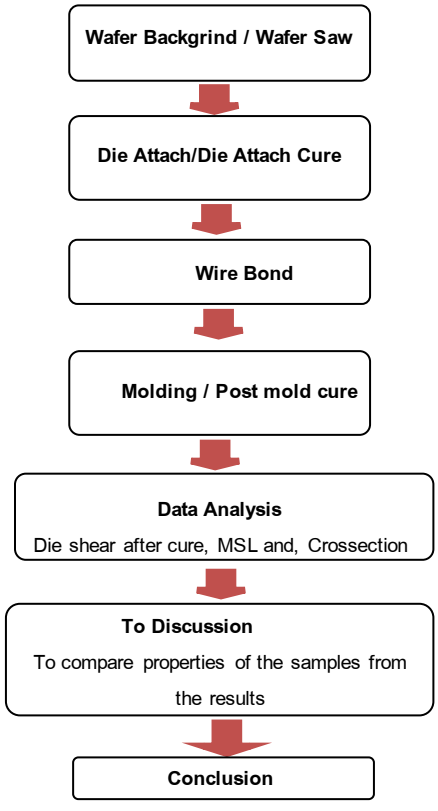

Figure 1 Diagram of operation.

Die Shear Test

Die Shear Testing is the process of determining the strength of adhesion of a semiconductor die to the package's die attach substrate by subjecting the die to a stress that's parallel to the plane of die attach substrate, resulting in a shearing stress between: 1) the die-die attach material interface; and 2) the die attach material-substrate interface as shown in Figure 2.

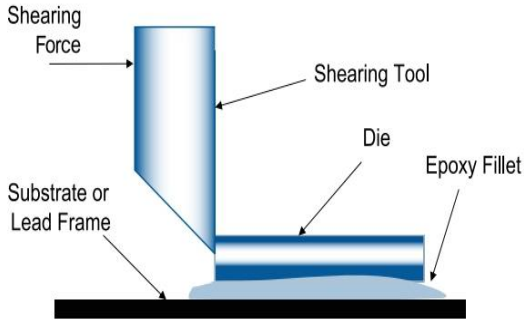

Figure 2 Die shear test.

Die shear strength is typically reported in kilogram and can significantly due to die and substrate composition as well as die size. For larger dies, lower stress material is recommended because of the greater surface area as shown in Table 2.

Table 2 The strong the bond.

High	> 10 kg / 3400	psi
Medium	5 - 10 kg / 1700 - 3400	psi
Low	< 2 - 5 kg / <1000	psi

Moisture Sensitive Level

The MSL is an electronic standard for the time period in which a moisture sensitive device can be exposed to ambient room conditions.

For moisture sensitivity level 1 (MSL 1) test, the procedures are shown in Figure 3 and Table 2.

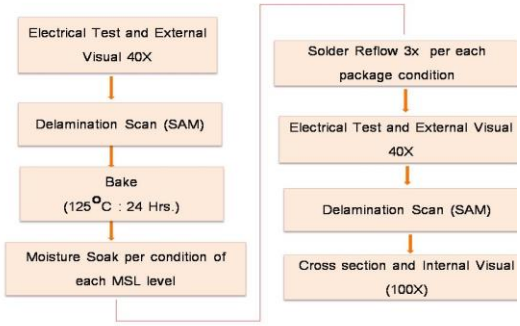

Figure 3 Procedure of moisture sensitivity level (MSL) test.

Table 2 Standard of moisture sensitivity level (MSL).

MSL	Floor life	
	Time	Condition
1	Unlimited	≤ 30 °C/85%RH
2	1 year	≤ 30 °C/60%RH
3	168 hrs	≤ 30 °C/60%RH

Cross Section

Cross-section is destructive technique offer a wealth of information about the IC device such as layer thicknesses, layer structures, grain sizes of various crystals in the layers and the existence of voids and delaminations.

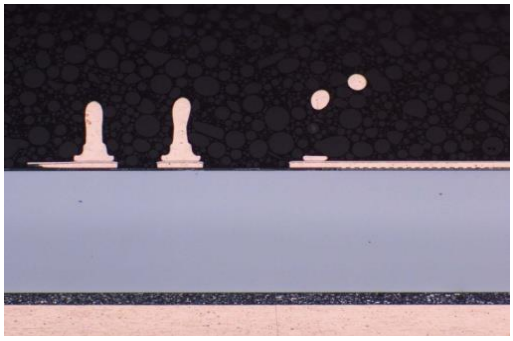

Figure 4 Procedure of Cross section.

Results and Discussion

Die Shear Test

The results of die shear strength after die attach cure. The die shear comparison between conventional oven cure and pressure oven cure. Therefore, conventional oven cure is higher than pressure oven cure as shown in Figures 5 and 6.

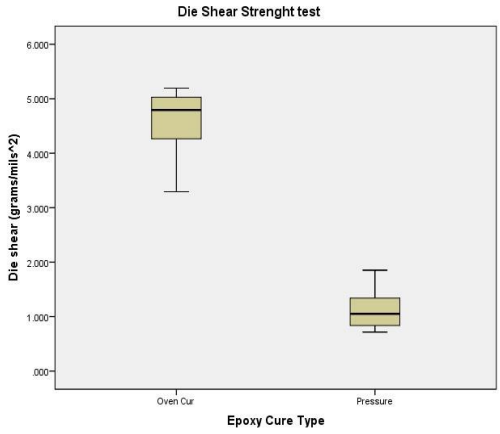

Figure 5 Die shear strength between Oven type.

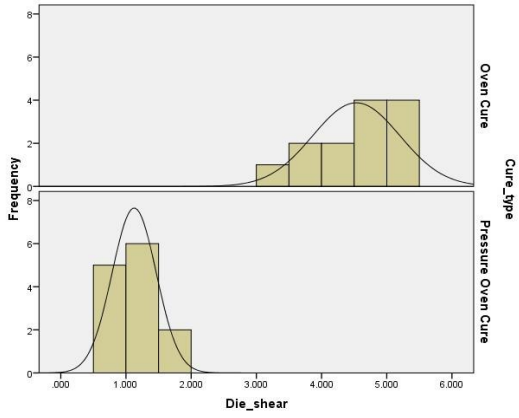

Figure 6 Die shear strength between Oven type.

Delamination Test

All the IC package was performed the delamination test to checking the delamination separation or internal void for conventional oven cure and pressure oven cure. The delamination test result shown no any delamination, separation and internal void.

Table 3 The delamination test result for oven cure.

Sample	Delamination test result	CSAM / TSAM Picture	
		CSAM	TSAM
1	0/22 No delamination	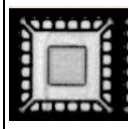	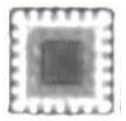
2	0/22 No delamination	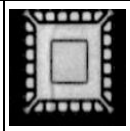	
3	0/22 No delamination	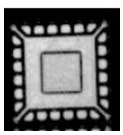	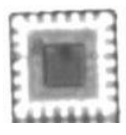
4	0/22 No delamination	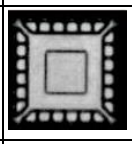	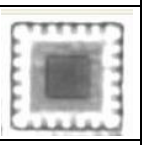
5	0/22 No delamination	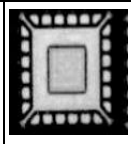	
6	0/22 No delamination	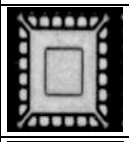	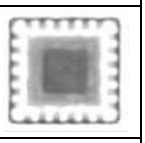
7	0/22 No delamination	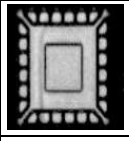	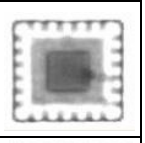
8	0/22 No delamination	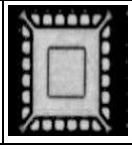	

Table 4 The delamination test result for pressure oven cure.

Conclusions

This research studied comparison between conventional oven cure and pressure oven cure. The die shear strength is a test conventional oven cure is higher than pressure oven cure. The delamination test result for conventional oven cure and pressure oven cure. Therefore, pressure oven cure used for reduction the void that has effect to the reliability of IC package

Acknowledgments

This research was supported by Utac Thai Limited, Mrs. Nantaporn Rattanasin and employees of Utac Thai Limited for recommendation and valuable comme.

References

[1] Su Y., et al. (2009). Effect of transfer pressure on die attach film void performance. *Proceeding of the 11th International Electronics Packaging Technology Conference.* 754-757.

[2] Sondag-Huethorst J.A.M. (2007). Dry film package for system in package molding process. *Proceeding of the 14th InternationalConference on Solid-State Sensors, Actuators and Microsystems*. 2071-2074.

[3] Ahmad I. (2007). Evaluation of different die attach film and epoxy pasters for stacked die QFN package. *Proceeding of the 9th Electronics Packaging Technology Conference*. 869-873.

[4] Song S.N. (2005). Die attach film appbication in multi die stack package. *Proceeding of the 11th International Electronics Packaging Technology Conference.* 848-852.

[5] Chung C.L. (2003). A Study on the Characteristic of UV cured Die-attach Films In Stack CSP (Chip Scale Package). *Proceeding of the 15th International Conference on Microelectronics.* 365-368.